

Understanding Experimental Facts for the Transformation of Perezone into α - and β -pipitzols

Luis Mauricio Murillo-Herrera^{1,2}, Fátima Soto-Suárez¹, Eduardo Hernández-Huerta¹, Karla Ramírez-Gualito³, Mariana Ortiz-Reynoso⁴, Ramiro F. Quijano-Quiñones^{5*}, Gabriel Cuevas^{1*}

¹Instituto de Química. Universidad Nacional Autónoma de México. Circuito Exterior, Ciudad Universitaria 04510, Coyoacán.

²Current address: Department of Chemistry, University of York, Heslington, York YO10 5DD, United Kingdom.

³Facultad de Ingeniería, Universidad Anáhuac México. Avenida Universidad Anáhuac 46, Col. Lomas Anáhuac, Huixquilucan, 52786, Estado de México, México.

⁴Facultad de Química, Universidad Autónoma del Estado de México, Paseo Colón esq. Paseo Tollocan. 50120, Residencial Colón, Toluca, Estado de México. México.

⁵Facultad de Química, Universidad Autónoma de Yucatán, Calle 43 No 613 por calle 90, Colonia Inalámbrica. 97069. Mérida, Yucatán, México.

*Corresponding author: Ramiro F. Quijano-Quiñones, email: ramiro.quijano@correo.uady.mx; Gabriel Cuevas, email: gecgb@unam.mx

Received December 11th, 2022; Accepted May 29th, 2023.

DOI: <http://dx.doi.org/10.29356/jmcs.v68i1.1926>

This paper is dedicated to Prof. Joaquín Tamariz Mascarua, who is an example of dedication oriented to the development of Mexican chemistry. He served as editor-in-chief of this Journal right around the time it acquired the impact index.

Abstract. Under thermal conditions perezone, a sesquiterpene quinone, forms an equimolar amount of α - and β -pipitzol through an intermolecular cycloaddition reaction. Computational calculations at M06-2x/6-311++G(2d,2p) level of theory of the transition states and the associated reaction paths allow justifying the experimental observations. Only *exo* adducts are observed experimentally, which is in line with the calculated energy difference of 6.5 kcal/mol between the transition states associated with the *endo* and *exo* adducts. Activation free energy was accurately predicted, those the uncatalyzed thermal process of cycloaddition requires 37.0 kcal/mol. The study of the potential energy surface allows to establish the existence of folded conformers of perezone in the potential energy surface.

Keywords: Perezone; α -pipitzol; β -pipitzol; reaction mechanism; concerted reaction.

Resumen. En condiciones térmicas la perezona, una quinona sesquiterpénica, forma, cantidades equimolares de α - y β -pipitzoles a través de una reacción de cicloadición intramolecular. A nivel M06-2x/6-311++G(2d,2p) el cálculo de los estados de transición y de las trayectorias de reacción asociadas permiten justificar los resultados observados. Desde el punto de vista experimental sólo se forman los aductos *exo* y no los *endo* pues los estados de transición relacionados muestran una diferencia energética de 6.5 kcal/mol. La energía de activación calculada para el procedo desprovisto de catálisis es de 37.0 kcal/mol. El estudio de la superficie de energía potencial permite establecer la existencia de conformeros plegados de la perezona.

Palabras clave: Perezona; α -pipitzol; β -pipitzol; mecanismo de reacción; reacción concertada.

Introduction

It is well known that depending on the time of year in which the pipitzahuac roots are collected, it is possible to isolate predominantly perezone [1] (**1**, Fig. 1) or a homogeneous mixture of α - (**2-a**) and β -pipitzols (**2-c**, Fig. 1) that naturally co-crystallize. [2-4] The extracts of this plant of the *Acourtia* genus have been used in traditional Mexican medicine since pre-Columbian times. The genus *Perezia* has been reconsidered as *Acourtia* and some synonyms for this plant are *Acourtia humboldtoii*, (BL Robinson & Green Reveal & RM King), formerly *Perezia cuernavacana* (BL Rob & Green), and initially *Trixis pipitzahuac*, (Schaff. Ex Herrera) Asteracea (Herrera).

In 1852 the Mexican pharmacist Leopoldo Río de la Loza isolated perezone in its crystalline form from a crude extract that had been provided to him by Pascual Díaz Leal by sublimation from the dried root, or by alcohol extraction followed by recrystallization from gasoline.[5] He reported the first elemental analysis developed in Mexico using the method implemented by Professor Justus von Liebig in Germany. [6] Río de la Loza analysis turned out to be erroneous, as a nitrogen atom was incorrectly assigned to the molecular formula, [7] nonetheless this assay should be considered a historical milestone, being the first attempt to carry out Liebig's method for organic elemental analysis in America.

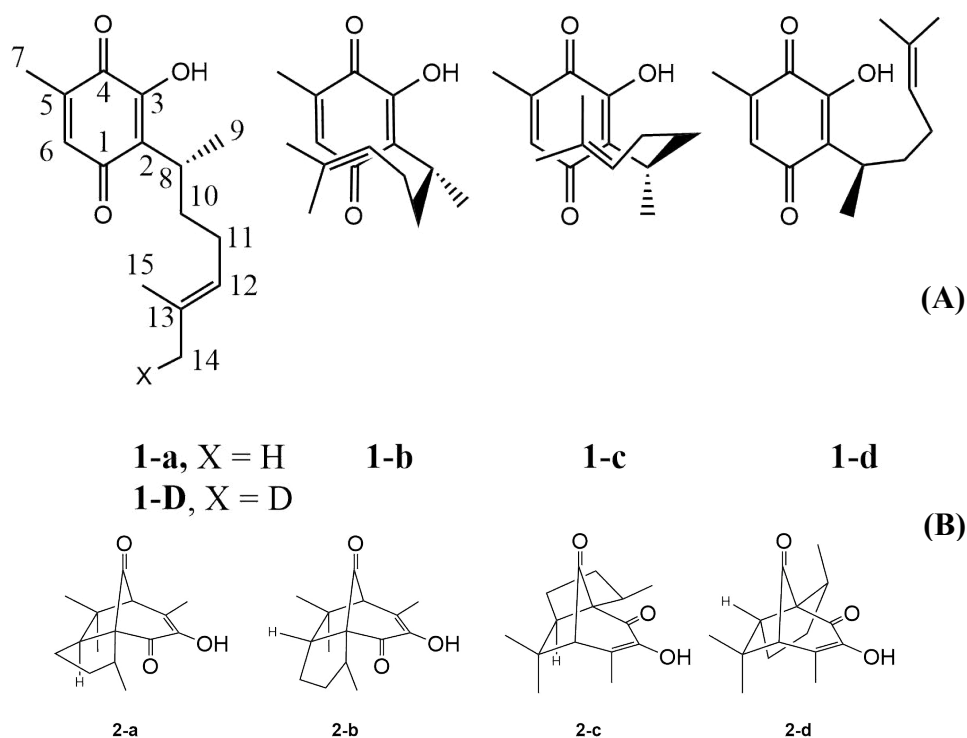


Fig. 1. (A) Perezone molecular structure with extended (**1-a** and **1-d**) and folded (**1-b** and **1-c**) conformers (See Fig. S1). (B) Four possible cycloaddition adducts: α -pipitzols (exo: **2-a** and endo: **2-b**) and β -pipitzols (exo: **2-c** and endo: **2-d**).

In 1857 Severiano Pérez reported the finding of a white and crystalline substance as a component of the pipitzahuac resin, which he initially called fructicosina and later pipitzahuina,[8,9] two ways for naming pipitzols that were lost over time. Pérez described the first isolation of pipitzols through the accidental thermal transformation of perezone, obtaining them as a crystalline by-product of its purification using sublimation, however, Pérez only described some physical properties and did not delve the molecular composition of this by product. Pérez considered that Río de la Loza's perezone was a mixture formed by pipitzoles contaminated by colored compounds that imparted its color to the mixture. A serious mistake.

At the turn of the century, Remfry[10] obtained pipitzols by a thermal reaction of perezone but it was until 1965 when the first mechanism for this transformation was proposed, [1,11] in order to support perezone's connectivity proposal, which resulted to be wrong. This mechanism, suggested the intermediation of a cyclobutane, followed by two alkyl group migrations for the formation of the pipitzols. [1]

The connectivity of prerezone (**1**) was established the same year when four independent works were published. By means of ^1H NMR analysis, it was finally established that the correct connectivity of quinone substituents exhibits a methyl group and a hydrogen atom on the same side of the quinone.[12-15] With the connectivity described, it was possible to report the first total synthesis of perezone.[16] The determination of the chemical structure of perezone allowed to propose an adequate mechanism for the formation of pipitzols, whose structure had been determined shortly before by Romo *et al.* [1] Initially they established that the product of the reaction consisted of a mixture of two diastereomers, in which all the stereogenic centers formed in the reaction had opposite configurations, but since the stereogenic center at C8 (of *R* configuration, Fig. 1) is kept constant, diastereoisomers are formed.

Experimentally, the selective oxidation of the methyl vinyl group at position 14, located *trans* with respect to the alkyl chain of **1** using selenium oxide, produced a pair of reaction products from which the aldehyde was isolated, and subsequently reduced with sodium borodeuteride and deoxygenated.[17] In this way, it was possible to prepare monodeuterated perezone at only one methyl group. When subjected to the thermal conditions of cycloaddition, pipitzols were formed, in which there were no scattering labels, so this mechanism was interpreted to correspond to a class B cycloaddition [$\pi 4s + \pi 2s$][18] or as a sigmatropic reaction of [1,9] order.[17] Furthermore, it was observed that in thermal conditions the proportion of the obtained pipitzols was similar, without induction of the stereogenic center. [17]

Because pipitzols have their biogenetic origin in perezone and both are natural products, their study is part of our interest in the terminal biogenesis of terpenes. [19,20]

Results and discussion

Concerted cycloaddition of perezone (**1**)

The folded conformers of perezone which are the precursors of pipitzols, present two easily differentiable arrangements according to the face of the quinone on which the side chain approaches, and each of them presents two possible orientations of the double bond; this is whether the side chain approaches *exo* (**1-a** and **1-c**, Fig. 2) or *endo* (**1-b** and **1-d**). It is important to notice that to date only compounds originating from the *exo* approach have been isolated from the plant and obtained by synthesis.[1-4,16,18] Deuterium labeling experimentation on perezone's C14 methyl group (structure **1-d**, Fig. 1), demonstrated complete preservation of deuterium on methyl C14 of the *endo* adduct, thus assuring the concerted mechanism nature.[16,21,22]

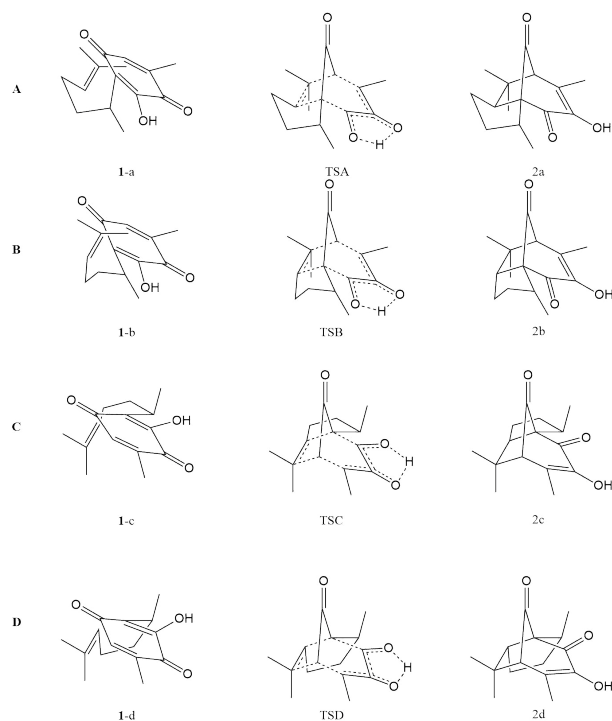


Fig. 2. Transition states in the formation of the four isomeric pipitzols **1-a** – **2-d**.

With the available conformers and the structure of the two isolable diastomeric pipitzols, the search for the transition states associated with the four possible approaches was undertaken. (See Table S3) All four transition states are characterizable and are presented in Fig. 3.

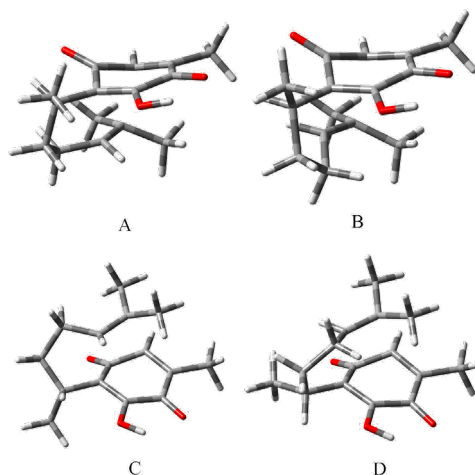


Fig. 3. Geometries of the transition-states **A**, **B** and **C**, **D** of the cycloaddition path to produce α - and β -pipitzols, respectively.

The mere existence of a transition state formally concludes the problem of the existence of the folded conformers of perezone as in this case, it has allowed the characterization of the four transition states associated with the formation of the four possible pipitzol diastereoisomers. On a surface of any nature, (potential energy in this case, and electron density or coulombic potential as an example), the existence of a point of (3, -1) curvature, (associable with a transition state) in which two curvatures are negative and one positive, the energy reaches a maximum within the plane defined by the corresponding axes and a minimum along the third axis which, is perpendicular to the previous plane. The existence of a transition state is a necessary and sufficient condition for the associated minima and maxima to exist, regardless of its vibrational nature.

The forming sigma bond distances and the pyramidalization (Δ) of the involved carbon atoms are presented in Table 1. In the transition state that leads to the formation of *exo*- β -pipitzol, the C2-C12 bond distance is the largest in all cases (see entry C, Table 1), while C6-C13 is the shortest. A larger bond could diminish the angular strain and allow for a more synchronous approximation of the two olefin carbon atoms towards the quinone center, affecting the experimented vibrational degrees of freedom. This can be understood in terms of the greater participation of the second bond in the stability (or the shorter length of the C6-C13 bond).

Table 1. Bond distances (\AA) and pyramidalization (Δ , in \AA) are associated to the formation of C2-C12 and C6-C13 bonds in their transition states.

Structure	DC ₂ -C ₁₂	DC ₆ -C ₁₃	Δ C ₂	Δ C ₁₂	Δ C ₆	Δ C ₁₃
A α -Exo	1.9956	2.1305	0.20378	0.12886	0.21279	0.17533
B α -Endo	2.0164	2.0856	0.15240	0.14404	0.18772	0.16608
C β -Exo	2.1398	2.0070	0.17319	0.12073	0.17573	0.14644
D β -Endo	1.9899	2.0946	0.14741	0.13233	0.16969	0.14645

Table 2 shows the energy parameters for the formation of the four possible products of cycloaddition using tetralin as an implicit solvent.[1] In terms of the stability of the adducts, the transition states that lead to the *exo* isomers are *ca.* 6.0 kcal/mol more stable than the *endo* ones, being enthalpy as the major contributor term. The angular strain on *endo* products, causes a stability loss reflected mainly on the enthalpic term, with values matching the T Δ S term (T = 480 K), while for the *exo* products the T Δ S term represents 40 % of the enthalpy value. Lastly, the *exo* adduct derived α - and β -pipitzols are 10.8 and 11.8 kcal/mol more stable with respect to their parent conformer.

Table 2. Kinetic and thermodynamic data for intramolecular cycloaddition [5 + 2] of perezone at 480 K, 1 atm and tetralin dielectric constant. The free energy (G) and enthalpy (H) values are in kcal/mol while those of entropy (S) are in cal/K·mol.

Reaction*	Kinetic data			Thermodynamic data		
	ΔH^\ddagger	ΔS^\ddagger	ΔG^\ddagger	ΔH°	ΔS°	ΔG°
A α -Exo	30.4	-14.5	37.4	-18.0	-15.0	-10.8
B α -Endo	36.6	-15.2	43.8	-7.4	-17.2	0.8
C β -Exo	32.5	-11.8	38.2	-19.0	-15.3	-11.8
D β -Endo	38.6	-12.3	44.4	-7.3	-12.9	-1.1

See Fig. 2

Data presented in Fig. 4, allowed us to quickly conclude on why, neither α - nor β - adducts generated by the side chain *endo* approximation have ever been observed. The activation energy for the former is 6.5 kcal/mol while for the latter is 6.3 kcal/mol higher with respect to the corresponding transition states for the formation of *exo* products. The formation of β -pipitzol requires overpassing an activation energy barrier of $\Delta G^\ddagger = 37.4$ kcal/mol, while for α -pipitzol this energy is of 38.3 kcal/mol. Therefore, a resulting energy difference of $\Delta\Delta G^\ddagger = 0.8$ kcal/mol led to an approximate proportion of 70/30. [23]

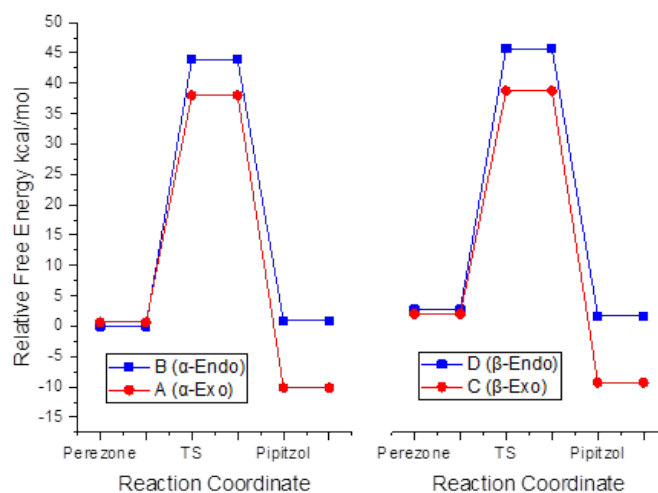


Fig. 4. Intramolecular [5+2] cycloaddition paths of perezone to produce α - and β -pipitzols at M06–2X/6-311++G(2d,2p) level of theory in tetralin as implicit solvent.

Activation enthalpy favors the formation of stable *exo* adducts, since angular strain is larger in *endo* adducts. Selectivity towards *exo* adducts can be explained in terms of steric compression. Careful observation of the *endo* adducts allows to identify a severe deformation in the environment at C12 carbon. The steric demand that the five-membered ring closure requires is responsible for hindering the *endo* isomers formation. These isomers have not been observed, not even by heating methods in which the vibrationally excited states would be feasible, as it has been proposed as mechanisms without the existence of folded conformers. [24]

The sigma bond formation process is asynchronous since the C2-C12 bond is shorter than the C6-C13 one and the stability of C13 is attributable to its tertiary carbocation character. Nevertheless, the pyramidization degree is larger on C6 than C2, as it is with the C13 and C12 pair, probably originated from the intense angular tension upon the formation of the second bond and the bicycle closure.

The stability of C13 is originated as well by the hyperconjugation arising from two vicinal hydrogen atoms oriented in such a way that σ_{C-H} is held perpendicular to the carbon atom plane. The hyperconjugation contribution to stability is not ideal since C13 has a certain degree of pyramidization.

The approximation of the lateral chain towards the quinone group is defined by the dihedral angle C1-C2-C8-C18, with values of 98.1° and 52.0° for the transition states of *exo* adducts A and C (which lead to the formation of α - and β -pipitzol), respectively and the *endo* adducts with values of 129.4° and 122.4° for B and D, respectively (Table 1). The lateral chain folding entails the consecutive *gauche* conformation along that segment, with an ideal dihedral angle of 60°. In this regard, the *endo* transition states show an intense twisting concerning *exo* ones. The C2-C8-C10-C12 dihedral angle has values of 30.8° and 30.5° for A and C, respectively and 24.5° and 12.4° for *endo* B and D transition states, respectively. Nevertheless, the C8-C10-C11-C12 segment has a more relaxed geometry in transition state A of 56.6°, while the same

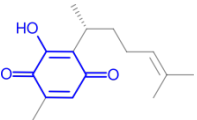
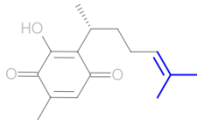
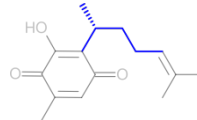
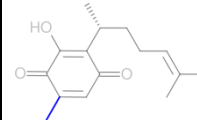
segment in transition state C shows a high degree of eclipsed conformation with a value of 3.9°. The same segment on B and D transition states show dihedral angles of 19.9° and 30.2° revealing the angular tension generated on these systems. Finally, the *endo* and *exo* orientations are described by the C10-C11-C12-C13 dihedral angle which has values of 152.5°, 133.4°, 157.6° and 160.5° for A, C, B and D transition states, respectively.

Topological analysis of the electron density

According to Professor Houk intermolecular interactions as well as deformations experimented by the reacting fragments in transition states determine both the favored products and the activation energies.[25] Since the fragments involved in the formation of pipitzols belong to the same molecule, carrying out deformation energy analysis is not possible. Instead, it was decided to obtain atomic properties under the framework of Bader's Quantum Theory of Atoms in Molecules (QTAIM).[26,27]

Table 3 shows the energetic differences corresponding to the evolution of 4 fragments of perezone: (F1) the quinoid ring, (F2) the isopropenyl group (F3) the alkyl chain bonding the first two, and (F4) the methyl group. The process comprises the change of the reagents to the corresponding transition states. This data indicates the isopropenyl group is responsible for the increase in energy required to reach the transition states of the 4 isomers. Charge transfer to the quinoid ring and pyramidalization accounts for the destabilization. The reduction in stability of F2 is compensated by the quinoid ring, which is increasingly stabilized when F2 approximates in *endo* fashion. The *exo* configuration, observed experimentally, is explained by the contributions of F3, since the steric compression which deforms the fragment is decisive as for the *exo* conformers, F3 is strongly stabilizing with contributions of -11.67 and -11.60 kcal/mol for the α - and β conformers respectively. The α -*endo* conformer is destabilizing with a contribution of 6.33 kcal/mol (18.00 kcal/mol overall with respect to the α -*exo* isomer). β -*endo* contribution of -2.64 kcal/mol is only slightly stabilizing. Hence, the steric compression of the lateral chain is decisive for the stereoselectivity of the *exo* isomers over the *endo*.

Table 3. Change in Potential Energy related to four fragments of perezone. Values in kcal/mol. (F indicates fragment)

					
	$\Delta\epsilon^\ddagger(\mathbf{F1})$	$\Delta\epsilon^\ddagger(\mathbf{F2})$	$\Delta\epsilon^\ddagger(\mathbf{F3})$	$\Delta\epsilon^\ddagger(\mathbf{F4})$	$\Delta\epsilon^\ddagger$
A α -Exo	-19.54	69.82	-11.67	-8.84	29.77
B α -Endo	-25.67	64.83	6.33	-6.65	38.85
C β -Exo	-19.57	70.15	-11.60	-9.24	29.74
D β -Endo	-25.10	72.22	-2.64	-6.36	38.12

Experimentally, the formation of α -pipitzol is similar to the formation of the β -isomer, in that the two adducts are obtained in the same proportion. The contributions to free energy show this behavior has its origin in the activation enthalpy, since in all cases the activation entropy maintains similar values and points towards the decrease of the well-known degrees of freedom common to cycloaddition reactions. Additionally, entropy is highly relevant for α -isomers with respect to β -isomers.

To study the influence of the steric clash as the energy barrier of the compounds studied here, a calculation of the non-covalent interactions (NCI) based on the reduced density gradient $s(r)$ was performed.

$$s(r) = \frac{1}{2(3\pi^2)^{1/3}} \frac{|\vec{\nabla}\rho(R)|}{\rho(r)^{4/3}}$$

The reduced density gradient $s(r)$ is a dimensionless quantity especially suited to identify noncovalent interactions that show the inhomogeneity of the electronic density. The capability of $s(r)$ to recognize chemical hallmarks is reflected by the positions of its critical points (CP). The CP in $s(r)$ is located at critical points in the electron density ($\nabla\rho(r)=0$), and at points where a complex balance between $\rho(r)$ and von Weizsäcker kinetic exists.[28] The latter are blind to QTAIM theory and correspond to intramolecular weak interactions. In this approach, the classification of the NCI is done in terms of the maximum variations in the contributions to the Laplacian, along with the axes, corresponding to the eigenvalues (λ_i) of the electron-density Hessian matrix. The sign of λ_2 enables us to distinguish between the different types of weak interactions, attractive and repulsive (such as steric repulsions), while the electron density lets us assess the interaction strength. To gain a deeper understanding of factors controlling the selectivity trends, we performed an analysis of NCI in TSs based on the study of the density reduced gradient.

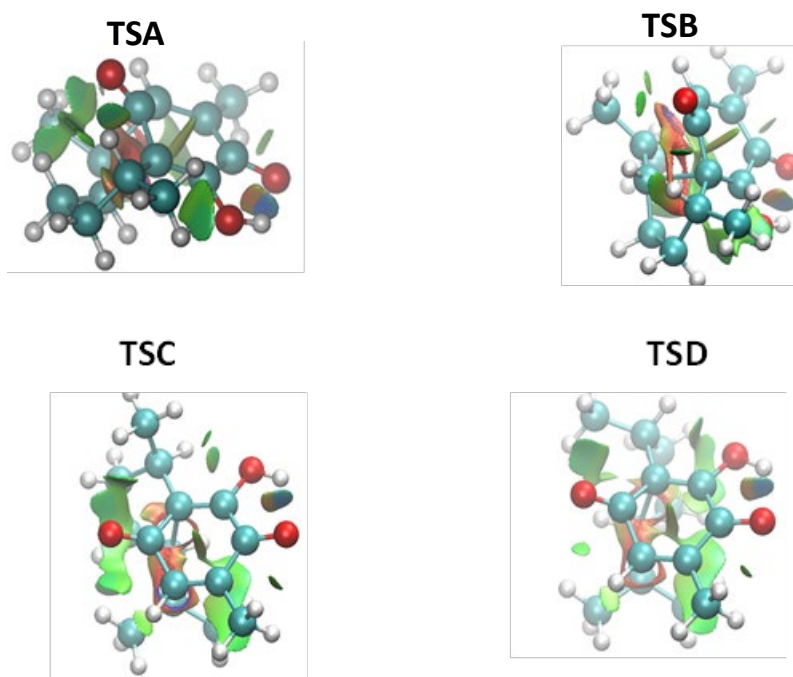


Fig. 5. Low gradient isosurfaces ($s=0.5$ u.a.) for the TS's in the thermal reaction.

Firstly, we considered the *endo-exo* selectivity in the thermal reaction to prove if the steric compression of the lateral chain is decisive for the stereoselectivity of the *exo* isomers over the *endo*, as is suggested by the atomic properties calculated using QTAIM.

Fig. 5 collects NCI surfaces of TSA, TSB, TSC, and TSD. We can observe a complicated group of NCI surfaces, where bicolored isosurfaces appear reflecting stabilizing features counter-balanced by destabilizing interactions due to steric crowding. Due to this complexity, it is not possible to point out that NCI is the cause of the observed selectivity. Therefore, we have performed an integration of the electronic density in NCI. The integration of the electronic density in volume elements, defined by $\text{sign}(\lambda_2)\rho$ ranges, has been proved to be a useful tool for the estimation of the strength of the NCI. [29] We performed the

integration of ρ in two ranges, corresponding to attractive ($-0.05 \leq \text{sign}(\lambda^2)\rho \leq 0.00$) and the repulsive ones ($0.00 \leq \text{sign}(\lambda^2)\rho \leq 0.05$). The results are depicted in Table 4.

Table 4. Repulsive and attractive electronic density integrals and their difference for TSs in the thermal reaction.

	$\iiint_{NCI} \rho(r) d\mathbf{v}$	
	Attractive	Repulsive
TSA	0.39	4.66
TSB	0.35	4.68
TSC	0.37	4.66
TSD	0.37	4.72

Analyzing the integral values for TSA and TSB in **Table 4**, it is clear that the attractive and repulsive NCI seems to govern the *endo-exo* selectivity. TSA presents the higher value of attractive NCI where the difference relative to TSB is equal to 0.04 u.a. On the other hand, the repulsive NCI integrals in the TSB are slightly higher than in the TSA case by 0.02 u.a. Therefore, we can conclude that both sorts of interaction lead the *exo* approximation as the preferred one. That is, in the *exo* TS the attractive NCI are maximized whereas the repulsive ones are slightly alleviated.

In the β -pipitzol case, the density integral values show that TSC present less steric repulsion than TSD with a difference of 0.06 u.a., whereas the value of the attractive density integral are the same. Therefore, these results allowed us to conclude that the *exo* preference in this instance is explained by the less steric hindrance in the *exo* approximation.

Methodology

All electronic structure calculations were performed under the Density Functional Theory (DFT) methodology, implemented in Gaussian09 software. [29] The stationary state geometries (reactants, transition states and products) were optimized using the meta-GGA M06-2X hybrid functional with the 6-311++G(2d,2p) Pople basis set; containing divided triple zeta valence and polarization functions on light and heavy atoms. M06-2x functional was employed since it has been recommended to study kinetics and thermochemical properties.[31] The geometry optimizations were carried out considering implicit solvent effects calculated with the SMD model along with the UAHF molecular cavity; tetraline solvent was employed for the thermal mechanism, while dichloromethane for the catalyzed mechanisms. Normal modes of vibration analysis allowed us to determine the nature of the stationary transition states (TS and energy minima displayed one and zero frequencies, respectively). Zero-point vibrational energy (ZPVE) and thermal corrections at 480 K (experimental conditions reported by J. Romo and coworkers[2] for the thermal mechanism). The intrinsic reaction coordinate (IRC) mapping was conducted in order to corroborate that transition structures were connecting the proposed minima. Changes in potential energy related to the different fragments of perezone were obtained through the topological analysis of the electron density of perezone using AIMAll software.[32] The NCI calculations were performed by means of a NCIPLLOT4 program,[29] and the resulting isosurfaces were visualized with the Visual Molecular Dynamics (VMD) software[34] following the next colour code: blue for attractive interactions, green for dispersive interactions (attractive or repulsive) and red for repulsive interactions.

Conclusions

Studying the concerted mechanism of perezzone transformation in to pipitzols, it is feasible to explain why only products originated from the *exo* approximation of the lateral chain have been described in the literature. The employed computational methodology at the M06-2X/6-311++G(2d,2p) level of theory allows establishing the selectivity of the reaction and the origin of the isotopic labelling distribution observed in the thermic process. The formation of *exo*-isomers with respect to the *endo* has its origin in the conformational arrangement of the side chain, which undergoes severe steric compression in the second case.

Acknowledgements

The authors are grateful to Gladys Cortés Romero and María Magdalena Aguilar Araiza, for technical assistance, we also thank the Dirección de Cómputo y de Tecnologías de Información y Comunicación of the Universidad Nacional Autónoma de México, via the grant LANCAD-UNAM-DGTIC-094, and to the Dirección General de Asuntos del Personal Académico (DGAPA) via grants No. IN-205620 and IN-208623. E R-L and FMSS. We are grateful to the Mexican Consejo Nacional de Ciencia y Tecnología (CONACYT) for the scholarship granted and also MM is grateful to the Sistema Nacional de Investigadores for sponsorship.

References

1. Walls, F.; Padilla, J.; Joseph-Nathan, P.; Giral, F.; Romo, J. *Tetrahedron Lett.* **1965**, 1577-1582. DOI: [https://doi.org/10.1016/S0040-4039\(01\)84094-6](https://doi.org/10.1016/S0040-4039(01)84094-6).
2. Walls, F.; Padilla, J.; Joseph-Nathan, P.; Giral, F.; Escobar, M.; Romo, J. *Tetrahedron.* **1966**, 22, 2387-2399. DOI: [https://doi.org/10.1016/S0040-4020\(01\)82159-1](https://doi.org/10.1016/S0040-4020(01)82159-1).
3. Evans, S.V.; Yee, V.C.; García-Garibay, M.A.; Trotter, J. *Acta Cryst.* **1994**, C50, 278-281. DOI: <https://doi.org/10.1107/S0108270193009060>.
4. Ylijoki, K.E.O.; Stryker, J.M. *Chem Rev.* **2013**, 113, 2244-2266. DOI: <https://doi.org/10.1021/cr300087g>.
5. Weld, M.C. *Ann. Ueber die Pipitzahöinsäure, eineneigenthümlichen Pflanzenstoff*, **1855**, 95, 188-192. DOI: <https://doi.org/10.1002/jlac.18550950205>.
6. Ortiz-Reynoso, M.; Cuevas González-Bravo G. E. *History of Pharmacy and Pharmaceuticals.* **2022**, 64, 154-186. DOI: <https://doi.org/10.3368/hopp.64.2.154>.
7. Rio de la Loza, L.; *Discurso pronunciado por el catedrático de Química Médica de la Escuela de Medicina el Noviembre 23, 1852. Periódico de la Escuela de Medicina.* **1853**, 1, 131-137.
8. a) Pérez, S. *Remitido. La Unión Médica.* **1857**, 2, 44-46. b) Jonás, A. *La Farmacia. En la Exposición Internacional de Filadelfia. Semanario Farmacéutico.* **1877**, 6, 5764.
9. Pérez, S. *La Farmacia.* **1890**, 1, No. 7. 101-107.
10. Remfry, F.G.P. *CXVI-Perezzone. J. Chem. Soc.* **1913**, 103, 1076-1088. DOI: <https://doi.org/10.1039/CT9130301076>.
11. Kögl, F.; Boer, A. G. *Rec. Trav. Chim.* **1935**, 54, 779-794. DOI:10.1002/recl.19350541005
12. Walls, F.; Salmón, M.; Padilla, J.; Joseph-Nathan, P.; Romo, J. *Bol. Inst. Quím. Univ. Nac. Auton. Mex.* **1965**, 17, 3-15.
13. Archer, D.A.; Thomson, R.H. *J. Chem. Soc. Chem. Commun.* **1965**, 354-355. DOI: <https://doi.org/10.1039/C19650000354>.
14. Bates, R.B.; Paknikar, S.K.; Thalacker, V.P. *Chem & Ind.* **1965**, 1793.
15. Wagner, E.R.; Moss, R.D.; Brooker, R.M. *Tet. Lett.* **1965**, 47, 4233-4239. DOI: [https://doi.org/10.1016/S0040-4039\(01\)89113-9](https://doi.org/10.1016/S0040-4039(01)89113-9).

16. a) Cortés, E.; Salmón, M.; Walls, F. *Bol. Inst. Quim. Univ. Nal. Autón. Méx.* **1965**, *17*, 19-33. b) Sánchez, I. H.; Larraza, M. I.; Basurto, F.; Yañez, R.; Avila, S.; Tovar, R.; Joseph-Nathan, P. *Tetrahedron*. **1985**, *41*, 2355-2359. DOI: [https://doi.org/10.1016/S0040-4020\(01\)96630-X](https://doi.org/10.1016/S0040-4020(01)96630-X).
17. Joseph-Nathan, P.; Mendoza, V.; García, E. *Tetrahedron*. **1977**, *33*, 1573-1576. DOI: [https://doi.org/10.1016/0040-4020\(77\)80163-4](https://doi.org/10.1016/0040-4020(77)80163-4).
18. Woodward, R.B.; Hoffman, R. in: *The Conservation of Orbital Symmetry*, Academic Press, New York, **1970**, 87. DOI: <https://doi.org/10.1002/anie.196907811>.
19. Barquera-Lozada, J.E.; Cuevas, G. *J. Org. Chem.* **2009**, *74*, 874-883. DOI: <https://doi.org/10.1021/jo802445n>.
20. Barquera-Lozada, J.E.; Quiroz-García B.; Quijano, L.; Cuevas, G. *J. Org. Chem.* **2010**, *75*, 2139-2146. DOI: <https://doi.org/10.1021/jo902170w>.
21. Aguilar-Martínez, M.; Bautista-Martínez, J. A.; Macías-Ruvalcaba, N.; González, I.; Tovar, E.; Marín del Alizal, T.; Collera, O.; Cuevas, G. *J. Org. Chem.* **2001**, *66*, 8349-8363. DOI: <https://doi.org/10.1021/jo010302z>.
22. Joseph-Nathan, P. in: *El deuterio, mi pequeño y valioso ayudante para estudiar productos naturales*, en Paredes-López, O.; Estrada-Orihuela, S (eds.) *Aportaciones científicas y humanísticas mexicanas en el siglo XX*. Fondo de Cultura Económica. **2008**, 435.
23. Lowry, T.H.; Richardson, K.S. in: *Mechanism and Theory in Organic Chemistry*, 2a. Ed., Harper & Row: New York. **1976**.
24. Zepeda, L.G.; Burgueño-Tapia, E.; Pérez-Hernández, N.; Cuevas, G.; Joseph-Nathan, P. *Reson. Chem.* **2013**, *51*, 245-250. DOI: <https://doi.org/10.1002/mrc.3940>.
25. Liu, F.; Paton, R.S.; Kim, S.; Liang, Y.; Houk, K.N. *J. Am. Chem. Soc.* **2013**, *135*, 15642–15649. DOI: <https://doi.org/10.1021/ja408437u>.
26. Bader, R. F. W. in: *Atoms in Molecules. A Quantum Theory*; Clarendon Press. Oxford, **1990**.
27. Keith, T.A., Version (13.11.04), TK Gristmill Software, Overlan, Oveland Park KS, USA **2013**.(aim.tkgristmill.com).
28. Joseph R. Lane, J. C.-G.; Piquemal, J.-P.; Miller, B. J.; Kjaergaard, H. G. *J. Chem. Theory Comput.* **2013**, *9*, 3263-3266. DOI: <https://doi.org/10.1021/ct400420r>.
29. Boto, R.A.; Peccati, F.; Laplaza, R.; Quan, C.; Carbone, A.; Piquemal, J.-P.; Maday, Y.; Contreras-García, J. *J. Chem. Theory Comput.* **2020**, *7*, 4150-4158. DOI: <https://doi.org/10.1021/acs.jctc.0c00063>.
30. Frisch, M.J.; Trucks, G. W.; Schlegel, H. B.; Scuseria, G. E.; Robb, M. A.; Cheeseman, J. R.; Scalmani G.; Barone, V.; Mennucci, B.; Petersson, G. A.; Nakatsuji, H.; Caricato, M. ; Li, X.; Hratchian, H. P.; Izmaylov, A. F.; Bloino, J.; Zheng, G.; Sonnenberg, J. L.; Hada, M.; Ehara, M.; Toyota, K.; Fukuda, R.; Hasegawa, J.; Ishida, M.; Nakajima, T.; Honda, Y.; Kitao, O.; Nakai, H.; Vreven, T.; Montgomery, J. A.; Peralta, J. E.; Ogliaro, F.; Bearpark M.; Heyd, J. J.; Brothers, E.; Kudin, K. N.; Staroverov, V. N.; Keith, T.; Kobayashi, R.; Normand, J.; Raghavachari, K.; Rendell, A.; Burant, J. C.; Iyengar, S. S.; Tomasi, J.; Cossi, M.; Rega, N.; Millam, J. M.; Klene, M.; Knox, J. E.; Cross, J. B.; Bakken, V.; Adamo, C.; Jaramillo, J.; Gomperts, R.; Stratmann, R. E.; Yazyev, O.; Austin, A. J.; Cammi, R.; Pomelli, C.; Ochterski, J. W.; Martin, R. L.; Morokuma, K.; Zakrzewski, V. G.; Voth, G. A.; Salvador, P.; Dannenberg, J. J.; Dapprich, S.; Daniels, A. D.; Farkas, O.; Foresman, J. B.; Ortiz, J. V.; Cioslowski, J.; Fox, D. J. *Gaussian 09*, Revision D.01, Gaussian, Inc., Wallingford CT, **2013**.
31. Zhao, Y.; Truhlar, D.G. *Acc. Chem. Res.* **2008**, *41* 157–167; DOI: <https://doi.org/10.1021/ar700111a>
32. Sánchez, I. H.; Yañez, R.; Enríquez, R. *J. Org. Chem.* **1981**, *46*, 2818-2819. DOI: <https://doi.org/10.1021/jo00326a052>.
33. Sánchez, I.H.; Basurto, F.; Joseph-Nathan, P. *J. Nat Prod.* **1984**, *47*, 382-383. DOI: <https://doi.org/10.1021/np50032a027>.
34. Humphrey, W.; Dalke, A.; Schulten, K. *J. Mol. Graphics.* **1996**, *14*, 33–38. DOI: [https://doi.org/10.1016/0263-7855\(96\)00018-5](https://doi.org/10.1016/0263-7855(96)00018-5).